A recommended modification to the dynamic two-parameter mixed subgrid scale model for large eddy simulation of wall bounded turbulent flow

Youhei Morinishi[a)]
Department of Mechanical Engineering, Nagoya Institute of Technology, Gokiso-cho, Showa-ku, Nagoya 466-8555, Japan

Oleg V. Vasilyev
Mechanical and Aerospace Engineering, University of Missouri-Columbia, E3415 Engineering Building East, Columbia, Missouri 65211

(Received 14 September 2000; accepted 31 July 2001)

It is well known that the correlation between the Smagorinsky model and the subgrid scale stress is low, while the model based on the scale similarity assumption has considerably higher correlation. However, the scale similarity model by itself was found to be insufficiently dissipative. Therefore, the model is usually used together with the Smagorinsky model. Model coefficients are commonly computed using the two-parameter dynamic procedure. Nevertheless, the dynamic two-parameter mixed model still does not work well for wall bounded flows, since the model predicts a high value of the wall shear stress. In this study, we propose a modification to the two-parameter dynamic procedure for wall bounded flows, which removes that defect: the Smagorinsky parameter, C_S, is computed exactly the same way as in the dynamic Smagorinsky model, then the other parameter, C_L, is computed dynamically as C_S is known. This ensures that the mixed model provides proper wall shear stress and mean velocity profile. Computational tests are done for turbulent channel flow where the Reynolds numbers based on the channel half-width and wall friction velocity are 395 and 1400. To remove the ambiguity regarding the accuracy of the finite difference scheme, we use high (up to 12th) order accurate fully conservative finite difference schemes in a staggered grid system.
 [DOI: 10.1063/1.1404396]

I. INTRODUCTION

The objective of this study is to present a modification to the dynamic two-parameter mixed model for large eddy simulation of wall bounded turbulent flow. It is well known that the correlation between the Smagorinsky model and the subgrid scale stress is low, while the model based on the scale similarity assumption by Bardina *et al.*[1] has considerably higher correlation (for example see Horiuti).[2] However, the scale similarity model by itself was found to be insufficiently dissipative. Therefore, the model is usually used together with the Smagorinsky model. Model coefficients are commonly computed using the dynamic procedure (Zang *et al.*,[3] Vreman *et al.*,[4] Salvetti and Banerjee,[5] Horiuti[6]). Nevertheless, the dynamic two-parameter mixed model still does not provide proper wall shear stress and mean velocity profile for wall bounded flows (Sarghini *et al.*[7]). In this study, we propose a modification to the two-parameter dynamic procedure, which removes this defect.

It is important to note that the defect of the scale similarity model is sometimes concealed when the large eddy simulation is performed with the standard second order finite difference scheme. The reliability of the results of large eddy simulation is strongly affected by both the reliability of the subgrid scale model and the accuracy of the numerical method (Ghosal[8]), particularly in the approximation of the convection term. This means that even if we use the exact subgrid scale stress, the computed flow field will be contaminated by the numerical error. This connection between the subgrid scale modeling and numerical error has been mostly overlooked. To remove the ambiguity regarding the accuracy of the finite difference scheme, we use mixed order fully conservative finite difference schemes in a staggered grid system proposed by Morinishi *et al.*,[9] where higher (up to 12th) order accurate discretization is used in homogeneous directions and second order accurate discretization with considerably higher resolution than that for the higher order scheme is used in wall normal direction. Computational tests are done in the turbulent channel flow and the Reynolds numbers based on the channel half-width and wall friction velocity are 395 and 1400.

The present paper is organized as follows. In Sec. II the basic equations of the large eddy simulation and existing dynamic subgrid scale models are introduced, and a recommended modification to the dynamic two-parameter mixed model is presented. In Sec. III the numerical method for the channel flow simulation is outlined. In Sec. IV computational results of the revised dynamic two-parameter mixed model are compared with those of the standard Smagorinsky, the dynamic Smagorinsky, and the standard dynamic two-parameter mixed model. The proposed modification to the dynamic two-parameter mixed model is justified there as well.

[a)]Author to whom correspondence should be addressed: electronic mail: morinisi@cfd.mech.nitech.ac.jp

II. BASIC EQUATIONS FOR THE LARGE EDDY SIMULATION AND SUBGRID SCALE MODELS

The basic equations for the large eddy simulation of incompressible flows are the filtered Navier–Stokes and continuity equations given by

$$\frac{\partial \overline{u_i}}{\partial t}+\frac{\partial \overline{u_i}\,\overline{u_j}}{\partial x_j}+\frac{\partial \tau_{ij}}{\partial x_j}=-\frac{\partial \overline{p}}{\partial x_i}+\nu\frac{\partial^2 \overline{u_i}}{\partial x_j\,\partial x_j}, \tag{1}$$

$$\frac{\partial \overline{u_i}}{\partial x_i}=0. \tag{2}$$

Here u_i is the velocity component in x_i direction ($i=1,2,3,$), p is the pressure divided by the density, ν is the kinematic viscosity, and t is time. The summation rule is assumed for repeated indices. The overbar $\overline{\cdot}$ denotes the filtering operator. $\overline{u_i}$ and $\overline{p}$ compose the resolved, grid scale (GS) flow field. $\tau_{ij}=\overline{u_iu_j}-\overline{u_i}\,\overline{u_j}$ is the subgrid scale (SGS) stress which should be modeled.

A. Dynamic Smagorinsky model

In the dynamic subgrid scale model, the identity of Germano *et al.*[10] between the grid and test fields is used to determine the parameter in the subgrid scale model

$$\mathcal{L}_{ij}=T_{ij}-\hat{\tau}_{ij}, \tag{3}$$

where the subtest stress T_{ij} is defined as $T_{ij}=\widehat{\overline{u_iu_j}}-\hat{\bar{u}}_i\hat{\bar{u}}_j$, and the resolved stress $\mathcal{L}_{ij}$ is defined as

$$\mathcal{L}_{ij}=\widehat{\overline{u_iu_j}}-\hat{\bar{u}}_i\hat{\bar{u}}_j. \tag{4}$$

In the standard dynamic subgrid scale model the Smagorinsky eddy viscosity model[11] is assumed for both the subgrid and subtest stresses:

$$\tau^*_{ij}=-2(C_S\overline{\Delta})^2|\overline{S}|\overline{S}_{ij},\quad \overline{S}_{ij}=\frac{1}{2}\left(\frac{\partial \overline{u_i}}{\partial x_j}+\frac{\partial \overline{u_j}}{\partial x_i}\right),$$

$$|\overline{S}|=(2\overline{S}_{ij}\overline{S}_{ij})^{1/2}, \tag{5}$$

$$T^*_{ij}=-2(C_S\hat{\Delta})^2|\hat{\bar{S}}|\hat{\bar{S}}_{ij},\quad \hat{\bar{S}}_{ij}=\frac{1}{2}\left(\frac{\partial \hat{\bar{u}}_i}{\partial x_j}+\frac{\partial \hat{\bar{u}}_j}{\partial x_i}\right),$$

$$|\hat{\bar{S}}|=(2\hat{\bar{S}}_{ij}\hat{\bar{S}}_{ij})^{1/2}. \tag{6}$$

The superscript "*" denotes the trace free operator ($\tau^*_{ij}\equiv\tau_{ij}-\frac{1}{3}\delta_{ij}\tau_{kk}$). The model parameter C_S is computed by minimizing the square of the error $Q=E_{ij}E_{ij}$ (Lilly[12]), where the error E_{ij} is given by

$$E_{ij}=\mathcal{L}^*_{ij}+2(C_S\overline{\Delta})^2M_{ij}, \tag{7}$$

$$M_{ij}=\alpha^2|\hat{\bar{S}}|\hat{\bar{S}}_{ij}-\widehat{|\overline{S}|\overline{S}_{ij}}, \tag{8}$$

and $\alpha^2=(\hat{\Delta}/\overline{\Delta})^2$ is the square value of the test to grid filter widths ratio. In this study we take $\alpha^2=5^{2/3}\sim 2.92$. It corresponds to[13] $\hat{\Delta}_1=\sqrt{5}\overline{\Delta}_1$, $\hat{\Delta}_2=\overline{\Delta}_2$, and $\hat{\Delta}_3=\sqrt{5}\overline{\Delta}_3$. Assuming C_S is a function of x_2 and taking the average in the x_1-x_3 plane (denoted by $\langle\cdot\rangle$) we obtain the following equation for $(C_S\overline{\Delta})^2$:

$$(C_S\overline{\Delta})^2=-\frac{1}{2}\frac{\langle\mathcal{L}_{ij}M_{ij}\rangle}{\langle M_{ij}M_{ij}\rangle}. \tag{9}$$

In this paper the dynamic Smagorinsky model given by Eqs. (5) and (9) is called DSM. In addition to this, the standard Smagorinsky model with the wall damping function[14] is used for comparison:

$$(C_S\overline{\Delta})=C_{S0}\left[1-\exp\left(-\frac{y^+}{25}\right)\right](\overline{\Delta}_1\overline{\Delta}_2\overline{\Delta}_3)^{1/3}, \tag{10}$$

where $\overline{\Delta}_i=h_i$ ($i=1,2,3,h_i$ are grid spacings), and $y^+=u_\tau y/\nu$ is the wall coordinate (y is the distance from the wall). Note that an alternative wall damping function can be used.[15] The model given by Eqs. (5) and (10) with $C_{S0}=0.10$ is called SM.

B. Dynamic two-parameter mixed model

The dynamic two-parameter mixed model of Salvetti and Banerjee[5] is based on the scale similarity model of Bardina *et al.*[1] and the Smagorinsky eddy viscosity model.[11]

$$\tau^*_{ij}=C_L(\widehat{\overline{u_i}\,\overline{u_j}}-\hat{\bar{u}}_i\hat{\bar{u}}_j)^*-2(C_S\overline{\Delta})^2|\overline{S}|\overline{S}_{ij}. \tag{11}$$

The two parameters, C_S and C_L, are computed by minimizing the square of the error $Q^{\mathrm{DTM}}=E^{\mathrm{DTM}}_{ij}E^{\mathrm{DTM}}_{ij}$, where the error E^{DTM}_{ij} is given by

$$E^{\mathrm{DTM}}_{ij}=\mathcal{L}^*_{ij}-C_L\mathcal{H}^*_{ij}+2(C_S\overline{\Delta})^2M_{ij}, \tag{12}$$

$$\mathcal{H}_{ij}=(\widehat{\hat{\bar{u}}_i\hat{\bar{u}}_j}-\hat{\bar{u}}_i\hat{\bar{u}}_j)-(\widehat{\overline{u_i}\,\overline{u_j}}-\hat{\bar{u}}_i\hat{\bar{u}}_j). \tag{13}$$

Following the standard procedure for the plane channel flow, the system for the two parameters is expressed as

$$\begin{bmatrix}A_{11} & A_{12}\\ A_{21} & A_{22}\end{bmatrix}\begin{bmatrix}C_L\\ 2C_S^2\end{bmatrix}=\begin{bmatrix}\langle\mathcal{L}_{ij}\mathcal{H}^*_{ij}\rangle\\ -\overline{\Delta}^2\langle\mathcal{L}_{ij}M_{ij}\rangle\end{bmatrix}, \tag{14}$$

where matrix **A** that appears in the left-hand side of Eq. (14) is given by

$$\begin{bmatrix}A_{11} & A_{12}\\ A_{21} & A_{22}\end{bmatrix}=\begin{bmatrix}\langle\mathcal{H}^*_{ij}\mathcal{H}^*_{ij}\rangle & -\overline{\Delta}^2\langle\mathcal{H}^*_{ij}M_{ij}\rangle\\ -\overline{\Delta}^2\langle\mathcal{H}^*_{ij}M_{ij}\rangle & \overline{\Delta}^4\langle M_{ij}M_{ij}\rangle\end{bmatrix}. \tag{15}$$

Solving the system Eq. (14), we obtain the following relations for C_L and $(C_S\overline{\Delta})^2$:

$$C_L=\frac{\langle\mathcal{L}_{ij}\mathcal{H}^*_{ij}\rangle\langle M_{ij}M_{ij}\rangle-\langle\mathcal{L}_{ij}M_{ij}\rangle\langle\mathcal{H}^*_{ij}M_{ij}\rangle}{\langle M_{ij}M_{ij}\rangle\langle\mathcal{H}^*_{ij}\mathcal{H}^*_{ij}\rangle-\langle\mathcal{H}^*_{ij}M_{ij}\rangle^2}, \tag{16}$$

$$(C_S\overline{\Delta})^2=-\frac{1}{2}\frac{\langle\mathcal{L}_{ij}M_{ij}\rangle\langle\mathcal{H}^*_{ij}\mathcal{H}^*_{ij}\rangle-\langle\mathcal{L}_{ij}\mathcal{H}^*_{ij}\rangle\langle\mathcal{H}^*_{ij}M_{ij}\rangle}{\langle M_{ij}M_{ij}\rangle\langle\mathcal{H}^*_{ij}\mathcal{H}^*_{ij}\rangle-\langle\mathcal{H}^*_{ij}M_{ij}\rangle^2}. \tag{17}$$

In this study, the dynamic mixed model given by Eq. (11) with coefficients C_L and $(C_S\overline{\Delta})^2$ determined by Eqs. (16) and (17) is called DTM.

C. Recommended modification to the dynamic two-parameter mixed model

The system for the least square problem, Eq. (14), is sensitive to the error on the right-hand side vector when the

condition number (the square root of the maximum to the minimum eigenvalues ratio) of matrix **A**, Eq. (15), is large. As will be shown later, the condition number is very large for the wall bounded flows and DTM does not provide appropriate wall shear stress. Therefore, DTM does not predict the mean velocity profile correctly. To remove this problem, we propose a modification to the dynamic two-parameter mixed subgrid scale model. A nearly ill-posed least square problem can be stabilized by introducing an approximation to matrix **A**. As it will be shown later, $|A_{21}| \ll |A_{22}|$ for the wall bounded flow and, consequently, matrix **A** can be approximated by the triangular matrix, which, in turn, leads to the following system of equations:

$$\begin{bmatrix} A_{11} & A_{12} \\ 0 & A_{22} \end{bmatrix} \begin{bmatrix} C_L \\ 2C_S^2 \end{bmatrix} = \begin{bmatrix} \langle \mathcal{L}_{ij} \mathcal{H}_{ij}^* \rangle \\ -\overline{\Delta}^2 \langle \mathcal{L}_{ij} M_{ij} \rangle \end{bmatrix}. \tag{18}$$

The second line of Eq. (18) gives the Smagorinsky parameter C_S exactly the same way as in DSM [Eq. (9)], and the resulting mixed model has enough SGS dissipation for GS turbulence energy. The other parameter can be stably computed as C_S is known:

$$C_L = \frac{\langle [\mathcal{L}_{ij} + 2(C_S \overline{\Delta})^2 M_{ij}] \mathcal{H}_{ij}^* \rangle}{\langle \mathcal{H}_{ij}^* \mathcal{H}_{ij}^* \rangle}. \tag{19}$$

Notice that system Eq. (18) still holds the condition of $\partial \langle Q^{\mathrm{DTM}} \rangle / \partial C_L = 0$. The revised dynamic mixed model given by Eq. (11) with Eqs. (9) and (19) is called DTMR.

III. NUMERICAL METHOD AND COMPUTATIONAL CASES

In this study the numerical tests for several subgrid scale models, described in the previous section, are performed using fully developed plane channel flow at Reynolds number of 395 and 1400. The flow field is assumed to be periodic in the streamwise (x_1) and spanwise (x_3) directions. The Reynolds number ($\mathrm{Re}_\tau = u_\tau H/\nu$) is based on the channel half-width H and the wall friction velocity u_τ. The treatment of the convection term [the second term on the left-hand side of Eq. (1)] is important for unsteady turbulent numerical simulations at high Reynolds number. Fully conservative higher (2nd, 4th, 8th, and 12th) order accurate finite difference schemes proposed by Morinishi *et al.*[9] are used for the convection term in the periodic directions. The second order accurate scheme with a volume weighted interpolation (Kajishima[16]) in the wall normal direction (x_2) (combined properly with higher order discretization in homogeneous directions) is used to remove the ambiguity regarding both the conservation properties of the nonuniform meshes and the wall boundary treatment.

The filtering operations in the dynamic subgrid scale models are done in the periodic directions. The test filtering with the filter width $\hat{\Delta}_i = 2h_i$ and the additional grid filtering with the filter width $\overline{\Delta}_i = h_i$ in x_i, $i = 1,3$, direction are done, respectively, as follows:

$$\hat{f}(x_i) = \tfrac{1}{6}[f(x_i - h_i) + 4f(x_i) + f(x_i + h_i)], \tag{20}$$

$$\overline{f}(x_i) = \tfrac{1}{24}[f(x_i - h_i) + 22f(x_i) + f(x_i + h_i)]. \tag{21}$$

TABLE I. Computational cases.

	Case 1	Case 2	Case 3	Case 4	Case 5
Re_τ	395				1400
L_1	$2\pi H$				
L_2	$2H$				
L_3	$2\pi H/3$				
N_1	24	32	48	64	96
N_2	64				96
N_3	24	32	48	64	96
h_1^+	103.4	77.6	51.7	38.8	91.6
h_2^+	$0.6 \sim 34.1$				$1.0 \sim 86.46$
h_3^+	34.5	25.9	17.2	12.9	30.5

A semi-implicit time marching method is used. The diffusion term in the wall normal direction is treated implicitly with the Crank–Nicolson method, and a third order Runge–Kutta (RK3) method of Spalart *et al.*[17] is used for all other terms. The splitting method by Dukowicz and Dvinsky[18] is used to enforce the solenoidal condition. The resulting discrete Poisson equation for the pressure is solved using a discrete Fourier transform in the periodic directions and a tridiagonal direct matrix solver in the wall normal direction. The time increments for the simulation at $\mathrm{Re}_\tau = 395$ and 1400 are $\Delta t = 2.5 \times 10^{-3}$ and 5.0×10^{-4}, respectively; these satisfy the stability condition for RK3.

Table I summarizes the grid resolution for all the computational cases in this study. The computational box for all the cases is $2\pi H \times 2H \times 2\pi H/3$. Cases 1–4 correspond to the flow at $\mathrm{Re}_\tau = 395$ and different grid resolutions in the periodic directions. Case 5 corresponds to the flow at higher Reynolds number $\mathrm{Re}_\tau = 1400$. The grid spacings in the periodic directions are uniform. The wall normal grid is stretched using a hyperbolic-tangent function

$$\frac{x_2(j)}{H} = \frac{\tanh[\gamma(2j/N_2 - 1)]}{\tanh[\gamma]}, \quad j = 0,...,N_2,$$

where $x_2(j)$ is the wall normal grid point for $\overline{u_2}$ in the staggered grid system and $x_2(0)$ and $x_2(N_2)$ correspond to the lower and upper walls, respectively. The stretching parameter, γ, is taken to be 2.75 and 2.95, respectively, for the flow at $\mathrm{Re}_\tau = 395$ and 1400.

IV. LES RESULTS AND DISCUSSION

A. Dependence of the LES result on the order of accuracy of the finite difference scheme and on grid resolution

Figures 1 and 2, respectively, show the effect of the order of the accuracy of finite difference scheme on the profiles

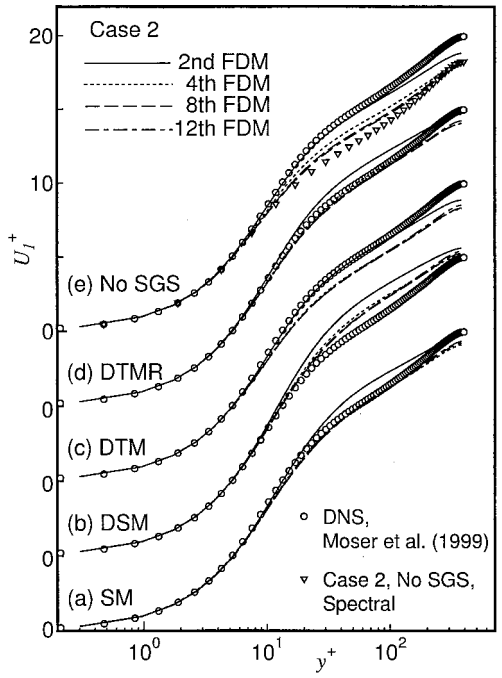

FIG. 1. The effect of the order of accuracy of the finite difference scheme on the mean streamwise velocity profile for the channel flow at $Re_\tau=395$ (Case 2) using SM, DSM, DTM, DTMR, and No SGS.

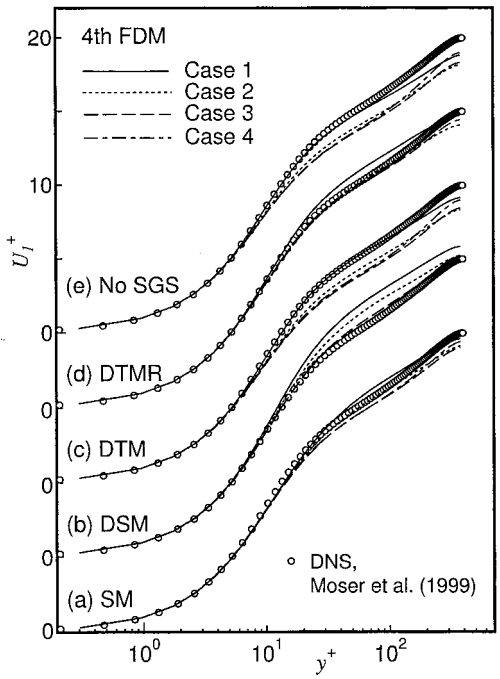

FIG. 3. The effect of grid resolution on the mean streamwise velocity profile for the channel flow at $Re_\tau=395$ using SM, DSM, DTM, DTMR, and No SGS with the fourth order accurate finite difference scheme.

of mean streamwise velocity U_1 ($U_1=\langle\overline{u_1}\rangle_t$) and streamwise grid scale velocity fluctuation u_1' ($u_1'=\sqrt{\langle\overline{u_1}^2\rangle_t-\langle\overline{u_1}\rangle_t^2}$) of the channel flow at $Re_\tau=395$ (Case 2) using SM, DSM, DTMR, and No SGS. The ensemble averaging over the x_1-x_3 plane and time is denoted by $\langle\cdot\rangle_t$. In the figures, variables with superscript "+" are normalized by the wall friction velocity u_τ and the viscous length scale δ_ν ($\delta_\nu=\nu/u_\tau$). The simulations without a subgrid scale model are labeled as No SGS. In these figures the DNS data by Moser *et al.*[19] are also plotted. The computational results with the 2nd, 4th, 8th, and 12th order accurate finite difference schemes in periodic directions are denoted, respectively, as 2nd, 4th, 8th, and 12th FDM. The results of a spectral (Fourier–Chebyshev) simulation corresponding to Case 2 without a subgrid scale model are also plotted in Figs. 1(e) and 2(e). Note that in the spectral simulation the wall normal grid distribution is different from that of Case 2 because the Gauss–Lobatto points are used. The discretization (or grid filtering) effect of the spectral method makes the mean velocity profile and the peak value of the velocity fluctuation lower than the DNS data, and the results of the higher order finite difference scheme are closer to the spectral one as shown in Figs. 1(e) and 2(e). In addition, the error of the second order scheme is considerably larger than those of the higher order schemes and shifts up the mean velocity profile and the peak value of the velocity fluctuation. This indicates that the discretization (grid filtering) effect of the finite difference scheme by itself makes the mean velocity profile lower than the DNS data, while the truncation error of the finite difference scheme acts as an effective subgrid scale stress and shifts up the mean velocity profile and the peak value of the velocity fluctuation. With an increase in the order of accuracy, the results using SM, DSM, DTM, and DTMR converge as shown in Figs. 1(a)–1(d) and 2(a)–2(d). It indicates that the effects of the truncation error are added to the results of the large eddy simulations. The mean velocity profile of DTM converges to a lower one than the DNS data with an increase in the order of accuracy, and the result of DTM with the second order scheme looks best in Fig. 1(c). However, the computational results with the second or-

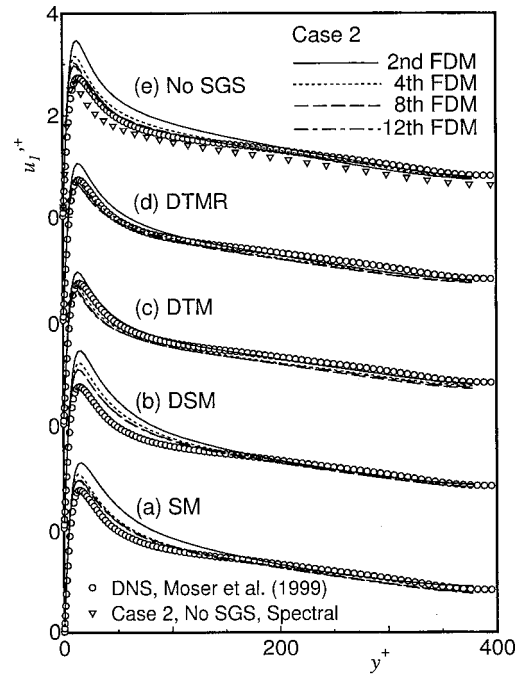

FIG. 2. The effect of the order of accuracy of the finite difference scheme on the streamwise grid scale velocity fluctuation profile for the channel flow at $Re_\tau=395$ (Case 2) using SM, DSM, DTM, DTMR, and No SGS.

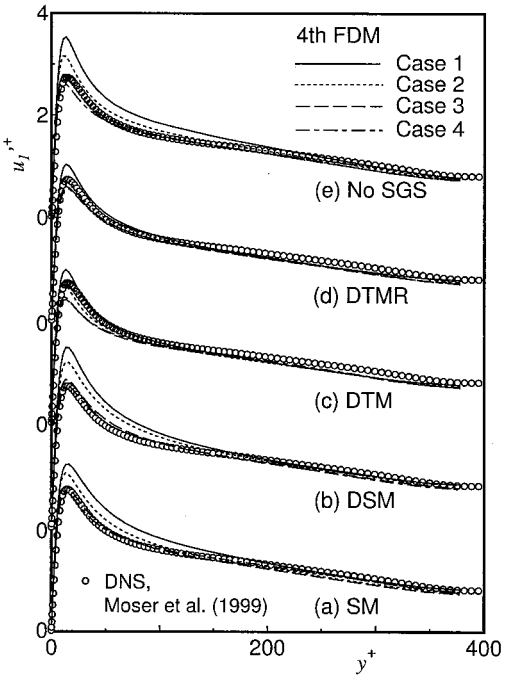

FIG. 4. The effect of grid resolution on the streamwise grid scale velocity fluctuation profile for the channel flow at $\mathrm{Re}_\tau=395$ using SM, DSM, DTM, DTMR, and No SGS with the fourth order accurate finite difference scheme.

der scheme are contaminated by large numerical error, and therefore, in order to estimate the subgrid scale models with the scheme, we would require considerably higher resolution than for higher order schemes.

Figures 3 and 4, respectively, show the effect of grid resolution on the profiles of the mean streamwise velocity and streamwise grid scale velocity fluctuation of the channel flow at $\mathrm{Re}_\tau=395$ using SM, DSM, DTMR, and No SGS with the fourth order finite difference scheme. The grid resolutions corresponding to Cases 1–4 are shown in Table I. With an increase in the grid resolution, the results of finite difference calculations converge. The numerical error of Case 1 is considerably larger than those of the finer resolution cases

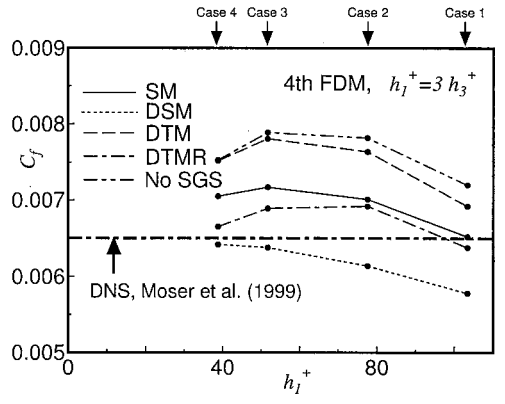

FIG. 5. The skin friction coefficient for the channel flow simulation at $\mathrm{Re}_\tau=395$ using SM, DSM, DTM, DTMR, and No SGS with the fourth order accurate finite difference scheme.

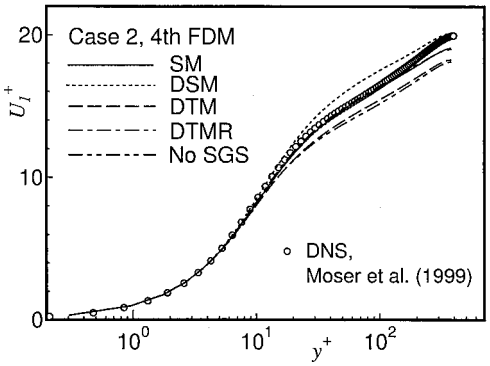

FIG. 6. The mean streamwise velocity profiles for the channel flow simulation at $\mathrm{Re}_\tau=395$ (Case 2) using SM, DSM, DTM, DTMR, and No SGS with the fourth order accurate finite difference scheme.

(Cases 2–4). The mean velocity profiles of SM, DSM, and DTMR converge to the DNS data with an increase in grid resolution, while the mean velocity profile of DTM converges to a lower one than the DNS result. This indicates that models SM, DSM, and DTMR have good asymptotic properties regarding grid resolution, while DTM does not.

Figure 5 shows the skin friction coefficient, $C_f=2\tau_w/(\rho U_m^2)$, for the cases which appeared in Fig. 3, where τ_w is the wall shear stress, ρ is the density, and $U_m=1/(2H)\int_{-H}^{+H}U_1\,dx_2$ is the bulk mean velocity. The C_f value of the DNS data by Moser *et al.*[19] is also plotted. The high intercept (constant B) of the log-law $[U_1^+=(1/\kappa)\ln y^+ +B]$ for DSM is due to the low value of the skin friction coefficient, while the low intercept of the log-law for DTM and No SGS is due to the high value of the skin friction coefficient.

B. Model comparison for Case 2 with the fourth order scheme

The effect of the subgrid scale model would be better estimated in numerical simulation with little or no numerical error. As demonstrated in the previous section, the large numerical error of the second order scheme makes it inappropriate for the model estimation. LES is considered to be a useful prediction tool for unsteady turbulent flow when direct numerical simulations are prohibitively expensive. This means that LES basically aims at simulations with relatively coarse grid resolution. Thus in this subsection, the performances of the subgrid scale models are checked using fourth order accurate finite difference scheme on a relatively coarse grid corresponding to Case 2.

Figure 6 shows the profiles of mean streamwise velocity using SM, DSM, DTM, DTMR, and No SGS. The difference between the mean velocity profiles for No SGS and the DNS results should be properly compensated by a subgrid scale model. The mean streamwise velocity profiles of the simulations using SM, DSM, and DTMR are shifted up when compared to the result of the simulation without a subgrid scale model. The profiles using SM and DTMR coincide well with the DNS data, while the mean velocity with DSM is too large. On the other hand, the two-parameter dynamic mixed model (DTM) does not compensate the difference properly, since the skin friction coefficient of DTM is almost the same

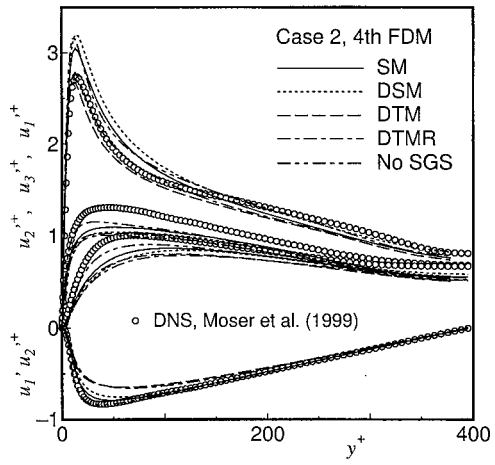

FIG. 7. The profiles of grid scale velocity fluctuations for the channel flow at $\mathrm{Re}_\tau=395$ (Case 2) using SM, DSM, DTM, DTMR, and No SGS with the fourth order accurate finite difference scheme.

as that of No SGS, as shown in Fig. 5. Figure 7 shows the profiles of grid scale velocity fluctuations ($u'_\alpha = \sqrt{\langle \overline{u}_\alpha^2 \rangle_t - \langle \overline{u}_\alpha \rangle_t^2}$, $\alpha=1,2,3$) and the grid scale Reynolds shear stress [$u'_1u'_2=\langle \overline{u}_1\overline{u}_2\rangle_t-\langle \overline{u}_1\rangle_t\langle \overline{u}_2\rangle_t$] using SM, DSM, DTM, DTMR, and No SGS. The peak value of the streamwise velocity fluctuation of the simulation without a subgrid scale model is higher than that of the DNS data. The defect of the finite difference simulation is not cured completely by the addition of the Smagorinsky models (SM and DSM). The streamwise velocity fluctuation of the DNS is not computed from the filtered field, and the rms fluctuations for the large eddy simulation should be smaller than or equal to the DNS data. The peak values of the streamwise velocity fluctuation obtained with the DTM and DTMR models are better than those obtained with the SM and DSM models.

Remember that the scale similarity model by itself was found to have insufficient SGS dissipation for GS turbulence energy, and therefore the model is used together with the Smagorinsky eddy viscosity model as the mixed model to remove the defect. Figure 8 shows the SGS dissipation profiles using SM, DSM, DTM, and DTMR. The C_S and C_L parts of the SGS dissipation are also plotted in the figure. The SGS dissipation that appears in the transport equation of GS turbulence energy [$k_{\mathrm{GS}}=\frac{1}{2}(\langle \overline{u_i}\overline{u_i}\rangle_t-\langle \overline{u_i}\rangle_t\langle \overline{u_i}\rangle_t)$] is given

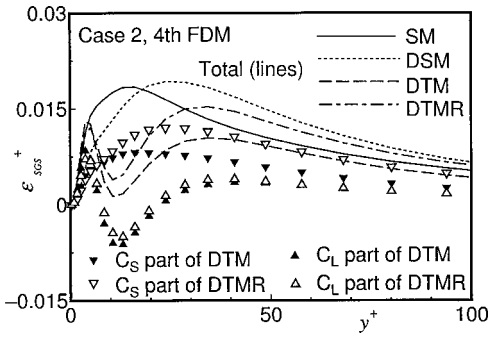

FIG. 8. The profiles of the SGS dissipation of the GS turbulence energy for the channel flow simulation at $\mathrm{Re}_\tau=395$ (Case 2) using SM, DSM, DTM, and DTMR with the fourth order accurate finite difference scheme.

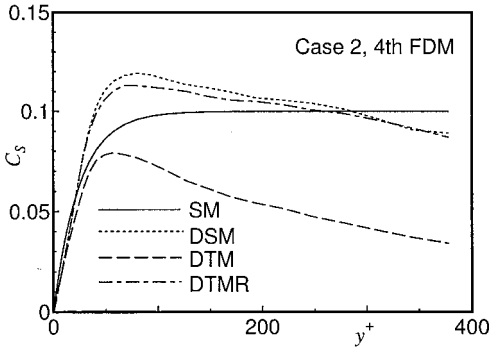

FIG. 9. The profiles of the model parameter C_S for the channel flow simulation at $\mathrm{Re}_\tau=395$ (Case 2) using SM, DSM, DTM, and DTMR with the fourth order accurate finite difference scheme.

by $\varepsilon_{\mathrm{SGS}}=-\langle \tau_{ij}\overline{S}_{ij}\rangle_t+\langle \tau_{ij}\rangle_t\langle \overline{S}_{ij}\rangle_t$. The different behavior of the SGS models is also reflected in different energy interchange mechanisms as was pointed out by Sarghini *et al.*[7] The bulk mean SGS dissipation, $\varepsilon^+_{\mathrm{SGS}_m}=1/(2H)\int_{-H}^{+H}\varepsilon^+_{\mathrm{SGS}}\,dx_2$, for SM, DSM, DTM, and DTMR are 3.87×10^{-3}, 4.53×10^{-3}, 2.58×10^{-3}, and 3.87×10^{-3}, respectively. The larger value of the bulk mean SGS dissipation corresponds to the smaller value of the skin friction coefficient. The DSM model is too dissipative and gives smaller skin friction and larger mean velocity as shown in Fig. 6. The DTM model is less dissipative, and yields the larger skin friction and smaller mean velocity. In particular, the C_L part of the dissipation is negative in the region around $y^+\sim10$. The C_S part of the dissipation is not enough and the defect of the scale similarity model is not cured if the model parameters are estimated through the dynamic procedure of DTM. The reason the defect is not cured by DTM is explained as follows: Horiuti[6] estimated the correlation coefficients between the exact subgrid scale stress computed from a DNS data and those obtained using different subgrid scale models and found that for the channel flow the correlation coefficient of DTM is 0.87–0.90, while the correlation coefficient of DSM is 0.03–0.35. This implies that the correlation of the scale similarity model to the exact subgrid scale stress is much higher than that of the Smagorinsky model. This unbalance makes C_S smaller if the two parameters are solved simultaneously. However, the low correlation of the Smago-

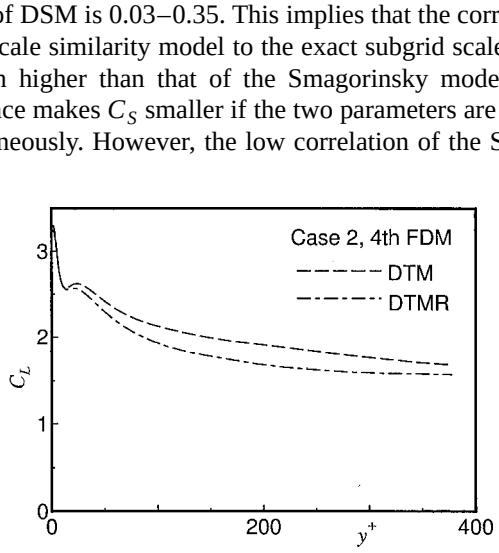

FIG. 10. The profiles of the model parameter C_L for the channel flow simulation at $\mathrm{Re}_\tau=395$ (Case 2) using DTM and DTMR with the fourth order accurate finite difference scheme.

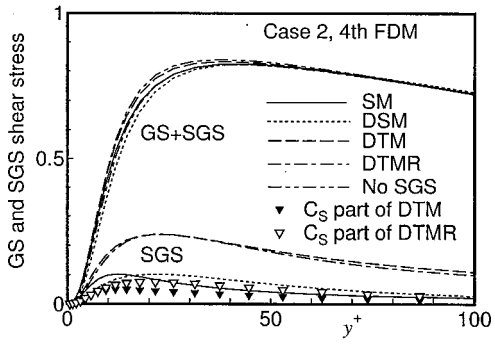

FIG. 11. The profiles of the effective Reynolds shear stress for the channel flow simulation at $Re_\tau=395$ (Case 2) using SM, DSM, DTM, and DTMR with the fourth order accurate finite difference scheme.

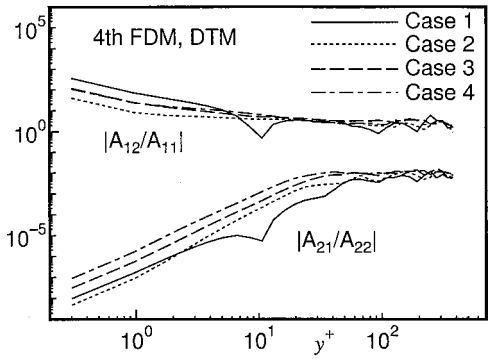

FIG. 13. The profiles of the element ratios $|A_{12}/A_{11}|$ and $|A_{21}/A_{22}|$ of matrix **A**, Eq. (15), for the channel flow simulation at $Re_\tau=395$ using DTM with the fourth order accurate finite difference scheme.

rinsky model also keeps C_L large even if the part of the scale similarity model is estimated later as in DTMR. The proposed modification makes use of this property.

Figures 9 and 10 show the profiles of the parameters C_S and C_L, respectively. The parameter C_S is plotted as $\mathrm{sign}[(C_S\overline{\Delta})^2]\sqrt{(C_S\overline{\Delta})^2/(h_1h_2h_3)^{2/3}}$. The profile, denoted as SM, shows the traditional C_S value with the wall damping function defined in Eq. (10). The C_S profile of DTMR is almost the same as that of DSM. The C_S value of DTM is much lower than that of DSM, DTMR, and the traditional value, and this results in smaller GS energy dissipation for DTM. The C_L profile of DTMR is almost the same as that of DTM, and the merit of the scale similarity model is kept in DTMR.

Figure 11 shows the profiles of the subgrid scale and the effective Reynolds shear stresses. The subgrid scale shear stress (τ_{12}^+) is denoted as SGS, and the C_S parts of the subgrid scale stress [the second term on the right hand side of Eq. (11)] of DTM and DTMR are also plotted as symbols in the figure. The effective Reynolds shear stress, i.e., the sum of the grid and subgrid scale shear stresses ($u_1'u_2'^+ + \tau_{12}^+$), is labeled as GS+SGS. Note that the order of the mean velocity profiles shown in Fig. 6 corresponds to the magnitude of the effective Reynolds shear stress close to the wall and does not follow the magnitude of the subgrid scale shear stress. It rather corresponds to the C_S part of the subgrid scale stress. This implies that the skin friction coefficient (and therefore the wall shear stress) is sensitive to the model parameter C_S, while it is passive to the model parameter C_L. This point will be elaborated later.

Figures 12 and 13, respectively, show the condition number and elements ratios ($|A_{12}/A_{11}|$ and $|A_{21}/A_{22}|$) for matrix **A**, Eq. (15). The condition number and the ratios are estimated by using an instantaneous flow field of DTM with the plane averaging. The condition number is very large near the wall, and the magnitude of A_{22} is considerably larger than A_{21}. These results support the basis of the revised procedure for wall bounded turbulent shear flows. In addition, the element A_{12} in Eq. (18) cannot be neglected with respect to A_{11}. Thus matrix **A** cannot be further approximated by the diagonal matrix. In the core region, since $C_S^2 \propto 0.01$, $C_L \propto 1$, and $|A_{21}/A_{22}| \propto 0.01$, A_{21} cannot be neglected with respect to A_{22}. This may restrict the application of the revised model to wall bounded turbulent flows.

C. Secondary effect of the Smagorinsky and scale similarity models

The addition of the subgrid scale stress model should reduce the mean velocity of the constant mean pressure gradient flow if the model does not act upon the grid scale fluctuating field. However, the discrete (or filtering) effect of

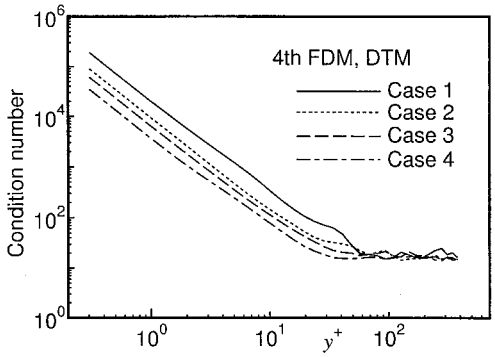

FIG. 12. The profiles of the condition number of matrix **A**, Eq. (15), for the channel flow simulation at $Re_\tau=395$ using DTM with the fourth order accurate finite difference scheme.

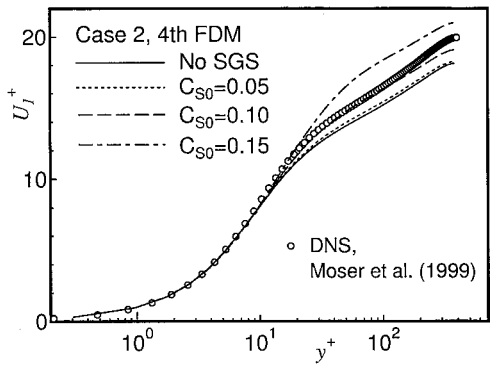

FIG. 14. The effect of the parameter C_{S0} of the Smagorinsky model [Eqs. (10) and (5)] on the mean streamwise velocity profile for the channel flow at $Re_\tau=395$ (Case 2) with the fourth order accurate finite difference scheme.

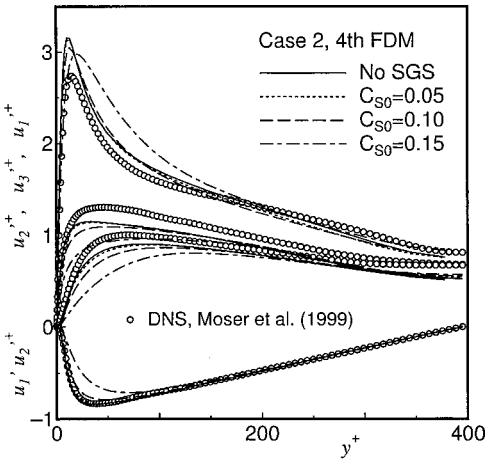

FIG. 15. The effect of the parameter C_{S0} of the Smagorinsky model [Eqs. (10) and (5)] on the grid scale velocity fluctuations for the channel flow at Re_τ=395 (Case 2) with the fourth order accurate finite difference scheme.

the finite difference method by itself reduces the mean velocity [for example, Fig. 1(e)], and the secondary effect of the model to increase the mean velocity is required for obtaining the proper mean velocity profile of the flow.

To illustrate the secondary effect of the Smagorinsky model, the simulations using Eq. (10) with different C_{S0} are performed. Figures 14, 15, and 16 show profiles of the mean streamwise velocity, the grid scale velocity fluctuations, and the effective Reynolds shear stress, respectively, for Case 2 with the fourth order finite difference scheme using Eqs. (10) and (5) with $C_{S0}=0.0$ (No SGS), 0.05, 0.10, and 0.15. The mean velocity increases and the spanwise and wall normal velocity fluctuations decrease with an increase in C_{S0}. The peak value of the streamwise velocity fluctuation is larger than the DNS data even for the case with $C_{S0}=0.15$. With an increase in C_{S0} the effective Reynolds shear stress decreases, while the subgrid scale shear stress increases. A decrease in the effective Reynolds shear stress yields an increase in the mean velocity. Figure 17 shows the corresponding SGS dissipation profile. The SGS dissipation increases with an increase in C_{S0}. The bulk mean SGS dissipations, $\varepsilon^+_{\mathrm{SGS}_m}$, for cases with $C_{S0}=0.05$, 0.10, and 0.15 are 1.28×10^{-3}, 3.84

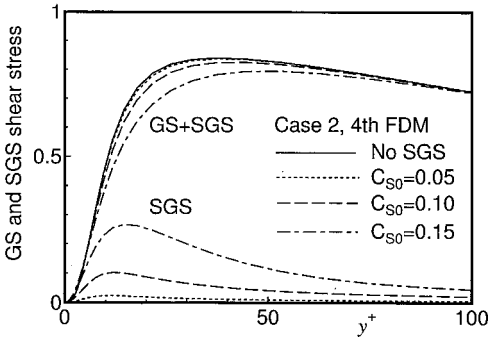

FIG. 16. The effect of the parameter C_{S0} of the Smagorinsky model [Eqs. (10) and (5)] on the effective Reynolds shear stress for the channel flow at Re_τ=395 (Case 2) with the fourth order accurate finite difference scheme.

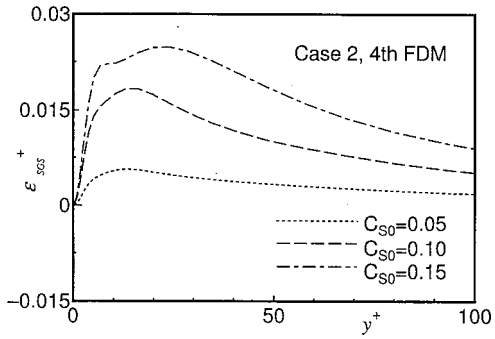

FIG. 17. The effect of the parameter C_{S0} of the Smagorinsky model [Eqs. (10) and (5)] on the SGS dissipation of the GS turbulence energy for the channel flow at Re_τ=395 (Case 2) with the fourth order accurate finite difference scheme.

$\times10^{-3}$, and 6.35×10^{-3}, respectively. An increase in the mean velocity in Fig. 14 corresponds to an increase in the bulk mean SGS dissipation.

In order to illustrate the secondary effect of the scale similarity model, we consider the model in Eq. (11) with $C_S=0$, i.e., the subgrid scale stress is approximated as

$$\tau^*_{ij}=C_L(\overline{\overline{u_iu_j}}-\bar{\bar{u}}_i\bar{\bar{u}}_j)^*. \tag{22}$$

Figures 18, 19, and 20, respectively, show the profiles of the mean streamwise velocity, grid scale velocity fluctuations, and the effective Reynolds shear stress for Case 2 with the fourth order finite difference scheme using Eq. (22) with $C_L=0.0$ (No SGS), 1.0, 2.0, and 4.0. The mean velocity decreases slightly and all velocity fluctuations decrease with an increase in C_L. The subgrid scale stress increases and the effective Reynolds shear stress increases slightly with an increase in C_L. An increase in the effective Reynolds shear stress yields a decrease in the mean velocity. Figure 21 shows the corresponding SGS dissipation profile. The profile has positive and negative extrema at $y^+=5$ and $y^+=10$, respectively, and the absolute values increase with increasing C_L. The bulk mean SGS dissipations, $\varepsilon^+_{\mathrm{SGS}_m}$, for the cases of $C_L=1.0$, 2.0, and 4.0 are 4.51×10^{-4}, 6.60×10^{-4}, and 8.32×10^{-4}, respectively. These values are much smaller than that of $C_{S0}=0.10$.

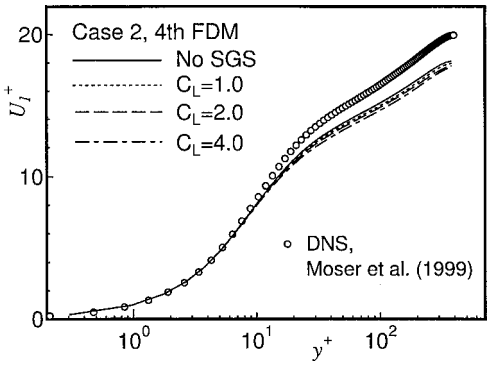

FIG. 18. The effect of the parameter C_L of the scale similarity model [Eq. (22)] on the mean streamwise velocity profile for the channel flow at Re_τ =395 (Case 2) with the fourth order accurate finite difference scheme.

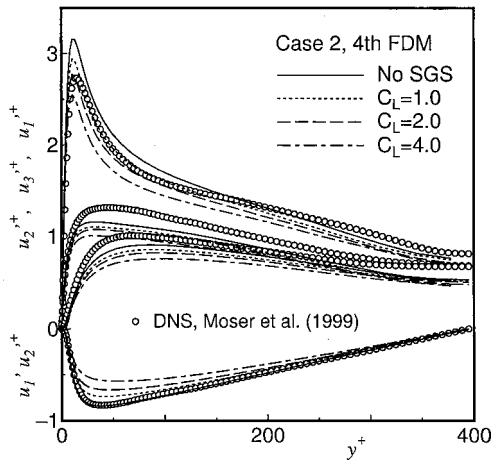

FIG. 19. The effect of the parameter C_L of the scale similarity model [Eq. (22)] on the grid scale velocity fluctuations for the channel flow at $\mathrm{Re}_\tau=395$ (Case 2) with the fourth order accurate finite difference scheme.

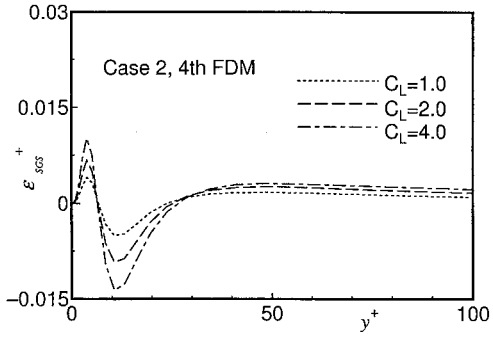

FIG. 21. The effect of the parameter C_L of the scale similarity model [Eq. (22)] on the SGS dissipation of the GS turbulence energy for the channel flow at $\mathrm{Re}_\tau=395$ (Case 2) with the fourth order accurate finite difference scheme.

Figure 22 shows the effect of the parameters of C_{S0} and C_L on the skin friction coefficient for the channel flow at $\mathrm{Re}_\tau=395$ (Case 2) with the fourth order accurate finite difference scheme. The C_f value of the DNS data by Moser *et al.*[19] is also plotted. The C_f value of the No SGS simulation ($C_{S0}=C_L=0$) is higher than the reference data, and yields the low intercept of the log-law (Figs. 14 and 18). The C_f value decreases with an increase in C_{S0}, and reaches the reference value at $C_{S0}\sim 0.12$, which is likely the optimal value of SM for Case 2 with the fourth order accurate finite difference scheme. On the other hand, the C_f value increases slightly with an increase in C_L, and it does not reach the reference value for $C_L>0$. Therefore the scale similarity model by itself cannot give the proper skin friction and mean velocity profile of the flow.

Summarizing the secondary effects of the subgrid scale models on the flow, the addition of the scale similarity model decreases slightly the mean velocity while that of the Smagorinsky model increases the mean velocity, and the scale similarity model is superior to the Smagorinsky model regarding the prediction of velocity fluctuations. In addition, the discrete effect of the finite difference method by itself reduces the mean velocity, while the truncation error of the finite difference scheme increases the mean velocity. The proposed model, DTMR, is a variant of DTM with the Smagorinsky part weighted, and is effective for the large eddy simulation of wall bounded turbulent flow when the effect of the truncation error is negligible.

D. The flow at a higher Reynolds number ($\mathrm{Re}_\tau=1400$, Case 5)

Figures 23 and 24 show the profiles of mean streamwise velocity and grid scale velocity fluctuations, respectively, using SM, DSM, DTM, DTMR, and No SGS at $\mathrm{Re}_\tau=1400$ (Case 5). The grid resolution of the simulation is shown in Table I and the fourth order finite difference scheme is used. In these figures the experimental data by Wei and Willmarth[20] are also plotted. The mean streamwise velocity profiles of the simulations with SM, DSM, and DTMR are shifted up when compared with the case of no subgrid scale model. The profiles using DSM and DTMR are closer to the experimental data. On the other hand, the difference between the profiles of DTM and No SGS is small, and the defect of DTM is apparent. The peak value of the computed streamwise velocity fluctuation without a subgrid scale model is higher than that of the experimental data. The defect of the

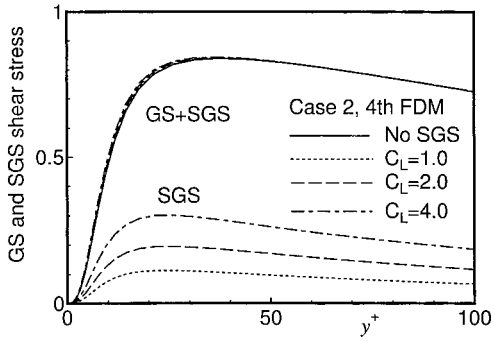

FIG. 20. The effect of the parameter C_L of the scale similarity model [Eq. (22)] on the effective Reynolds shear stress for the channel flow at $\mathrm{Re}_\tau=395$ (Case 2) with the fourth order accurate finite difference scheme.

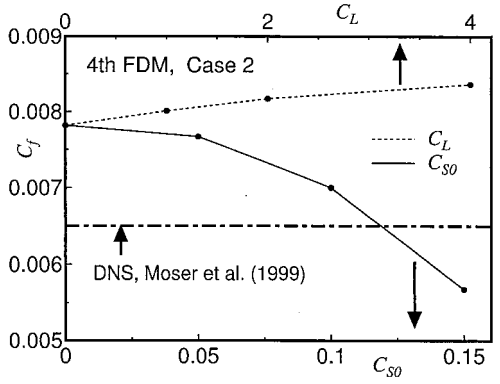

FIG. 22. The effect of the parameter C_{S0} and C_L on the skin friction coefficient for the channel flow at $\mathrm{Re}_\tau=395$ (Case 2) with the fourth order accurate finite difference scheme.

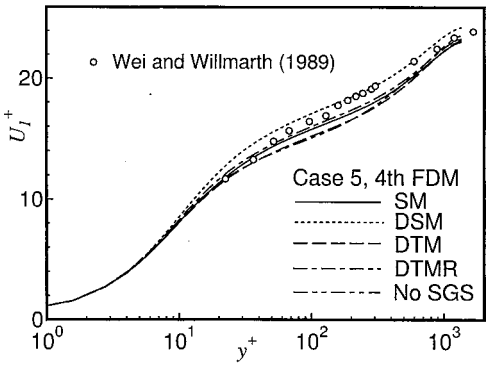

FIG. 23. The mean streamwise velocity profiles for the channel flow simulation at $Re_\tau=1400$ (Case 5) using SM, DSM, DTM, DTMR, and No SGS with the fourth order accurate finite difference scheme.

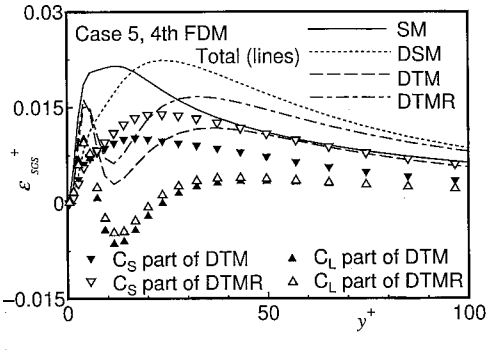

FIG. 25. The profiles of the SGS dissipation of the GS turbulence energy for the channel flow at $Re_\tau=1400$ (Case 5) using SM, DSM, DTM, DTMR, and No SGS with the fourth order accurate finite difference scheme.

finite difference simulation is not cured completely by the addition of the Smagorinsky models (SM and DSM). The peak values of the streamwise velocity fluctuation obtained with the DTM and DTMR models are better than those of the Smagorinsky models. Figure 25 shows the SGS dissipation profile using SM, DSM, DTM, and DTMR. The profiles of Case 5 are similar to those of Case 2 (Fig. 8). The bulk mean SGS dissipation, $\varepsilon^+_{\mathrm{SGS}_m}$, for SM, DSM, DTM, and DTMR are 2.05×10^{-3}, 2.29×10^{-3}, 1.48×10^{-3}, and 2.16×10^{-3}, respectively. It indicates that the DTM model does not have enough dissipation. From these results it is apparent that the revised model keeps the merit of both the eddy viscosity and the scale similarity subgrid scale models even for the high Reynolds number flow.

V. CONCLUSIONS

The dynamic two-parameter mixed model was expected to have the merits of both the Smagorinsky and scale similarity models, since it was constructed as a linear combination of two of them. The strength of the scale similarity model is that the correlation of the model to the subgrid scale stress is much higher than that of the Smagorinsky model. On the other hand, the secondary effect of the scale similarity model increases the skin friction and reduces the mean velocity of the turbulent channel flow, while that of the Smagorinsky model reduces the skin friction and increases the mean velocity. The filtering effect by itself increases the skin friction and reduces the mean velocity, and the secondary effect of a subgrid scale model to increase the mean velocity is required in order to obtain the proper mean velocity profile for the turbulent shear flow. Therefore, for the wall bounded flows the secondary effect of the Smagorinsky model improves the prediction of the mean velocity profile, while the secondary effect of the scale similarity model results in the deterioration of the mean velocity profile. The defect of the scale similarity model is emphasized when the two parameters are computed simultaneously through the standard dynamic procedure. We have proposed a modification to the two-parameter dynamic procedure for wall bounded turbulent flows, which removes that defect: the Smagorinsky parameter, C_S, is computed exactly the same way as in the dynamic Smagorinsky model, then the other parameter, C_L, is computed dynamically as C_S is known. This ensures that the mixed model gives proper skin friction and then yields reliable mean velocity profiles while keeping the merit of the scale similarity model. The reliability of the revised mixed model was confirmed by performing large eddy simulations of turbulent channel flow at the two Reynolds numbers $Re_\tau=395$ and 1400.

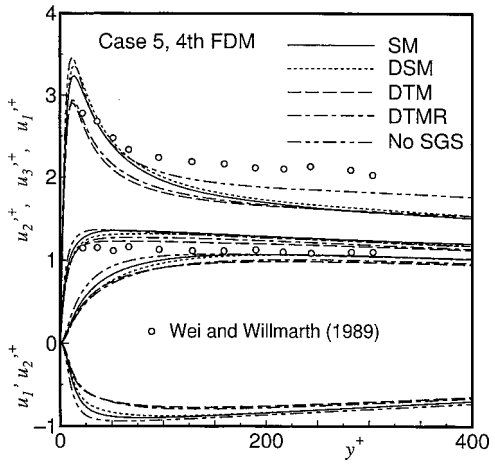

FIG. 24. The profiles of grid scale velocity fluctuations for the channel flow at $Re_\tau=1400$ (Case 5) using SM, DSM, DTM, DTMR, and No SGS with the fourth order accurate finite difference scheme.

ACKNOWLEDGMENTS

The authors thank Professor Parviz Moin for his support and continued interest in this work. Y.M. was partially supported by a Grant-in-Aid from the Ministry of Education, Science and Culture, Japan (No. 11750138), and also partially supported by Center for Promotion of Computational Science and Engineering, Japan Atomic Energy Research Institute. O.V. was supported by the University of Missouri Research Board Grant. In addition, the authors are grateful to two referees for useful suggestions.

[1]J. Bardina, J. H. Ferziger, and W. C. Reynolds, "Improved turbulence models based on large eddy simulation of homogeneous, incompressible, turbulent flows," *Stanford University Tech. Rep*. TF-19 (1983).

[2]K. Horiuti, ''The role of the Bardina model in large eddy simulation of turbulent channel flow,'' Phys. Fluids A **1**, 426 (1989).
[3]Y. Zang, R. L. Street, and J. R. Koseff, ''A dynamic subgrid-scale model and its application to turbulent recirculating flows,'' Phys. Fluids A **5**, 3186 (1993).
[4]B. Vreman, B. Geurts, and H. Kuerten, ''On the formulation of the dynamic mixed subgrid-scale model,'' Phys. Fluids A **6**, 4057 (1994).
[5]M. Salvetti and S. Banerjee, ''*A priori* tests of a new dynamic subgrid-scale model for finite-difference large-eddy simulations,'' Phys. Fluids A **7**, 2831 (1995).
[6]K. Horiuti, ''A new dynamic two-parameter mixed model for large-eddy simulation,'' Phys. Fluids A **9**, 3443 (1997).
[7]F. Sarghini, U. Piomelli, and E. Balaras, ''Scale-similar models for large-eddy simulations,'' Phys. Fluids **11**, 1596 (1999).
[8]S. Ghosal, ''An analysis of numerical error in large-eddy simulation of turbulence,'' J. Comput. Phys. **125**, 187 (1996).
[9]Y. Morinishi, T. S. Lund, O. V. Vasilyev, and P. Moin, ''Fully conservative higher order finite difference schemes for incompressible flow,'' J. Comput. Phys. **143**, 90 (1998).
[10]M. Germano, U. Piomelli, P. Moin, and W. H. Cabot, ''A dynamic subrid-scale eddy viscosity model,'' Phys. Fluids A **3**, 1760 (1991).
[11]J. Smagorinsky, ''General circulation experiments with the primitive equations. I. The basic experiment,'' Mon. Weather Rev. **91**, 99 (1963).
[12]D. K. Lilly, ''A proposed modification of the Germano subgrid scale closure method,'' Phys. Fluids A **4**, 633 (1992).
[13]B. Vreman, B. Geurts, and H. Kuerten, ''Large-eddy simulation of the turbulent mixing layer,'' J. Fluid Mech. **339**, 357 (1997).
[14]E. R. Van Driest, ''On turbulent flow near a wall,'' J. Aeronaut. Sci. **23**, 1007 (1956).
[15]U. Piomelli, J. H. Ferziger, and P. Moin, ''Models for large eddy simulations of turbulent channel flows including transpiration,'' *Stanford University Tech. Rep*. TF-32 (1987).
[16]T. Kajishima, ''Finite-difference method for convective terms using non-uniform grid,'' Trans. Jpn. Soc. Mech. Eng. **607–633B**, 607 (1999) [in Japanese].
[17]P. Spalart, R. Moser, and M. Rogers, ''Spectral methods for the Navier–Stokes equations with one infinite and two periodic directions,'' J. Comput. Phys. **96**, 297 (1991).
[18]J. K. Dukowicz and A. S. Dvinsky, ''Approximation as a higher order splitting for the implicit incompressible flow equations,'' J. Comput. Phys. **102**, 336 (1992).
[19]R. D. Moser, J. Kim, and N. N. Mansour, ''Direct numerical simulation of turbulent channel flow up to Re_τ=590,'' Phys. Fluids A **11**, 943 (1999).
[20]T. Wei and W. W. Willmarth, ''Reynolds-number effect on the structure of a turbulent channel flow,'' J. Fluid Mech. **204**, 57 (1989).